DISPERSE

Electronics for spatially distributed sensors and transducers arrays

Labelled in PENTA, a EUREKA cluster, Call 1

PENTA Project Number 16012

D2.4 Prototypes for multi-implant assessment, including bench test and EM simulation with typical lead routing

Due date of deliverable: M24

Start date of project: 1 February 2017	**Duration:** 36 months
Organisation name of lead contractor for this deliverable:	G-Therapeutics
Author(s):	Edoardo Paoles (G-Therapeutics)
Status:	Final
Version number:	1.0
Submission Date:	14-March-2019
Doc reference:	DISPERSE_Deliverable_D2.4_Prototypes for multi-implant assessment_V1.0
Work Pack./ Task:	Work package 2, Task 2.2 and 2.3
Description: ***(max 5 lines)***	This document describes the demonstrators realised in WP2 of the DISPERSE project.

Nature:	**Demo**		
Dissemination Level:	**PU**	Public	**X**
	PP	Restricted to other programme participants	
	RE	Restricted to a group specified by the consortium	
	CO	Confidential, only for members of the consortium	

DOCUMENT HISTORY

Release	Date	Reason of change	Status	Distribution
V0.1	24/01/2019	First draft	Draft	Edoardo Paoles
V0.2	28/02/2019	Added more information related to experimental work	Draft	Guy Fierens
V0.3	06/03/2019	Added sections 2, 3.1, 3.3 and 4	Draft	Edoardo Paoles
V0.4	11/03/2019	Added comments from KULeuven	Draft	Edoardo Paoles
V0.5	13/03/2019	Added executive summary and conclusion	Draft	Edoardo Paoles
V1.0	14/03/2019	Approved by PMT	Final	All

Table of Contents

Glossary

Abbreviation / acronym	Description
MRI	Magnetic Resonance Imaging
AIMD	Active Implantable Medical Device
RF	Radiofrequency
ASTM	American Section of the International Association for Testing Materials
GTX	G-Therapeutics
SCS	Spinal Cord Stimulator
MEI	Middle ear implant
HPM	High permittivity medium

1. Executive Summary

This document describes the demonstrators realised in WP2 of the DISPERSE project. In this work package prototypes for multi-implant assessment are developed. Specifically, GTX SCS system and Cochlear™ Carina® implant are presented. The interaction of the two implants within an MRI scanner for RF heating and image distortion is evaluated both in-silico (i.e. simulations) and in-vitro (i.e. phantom experiments). Results of bench tests are not available yet and will be discussed in another document.

2. Introduction

State-of-the-art MR conditional implant testing only considers the individual implant under test in the environment of an MRI scanner. Within DISPERSE we investigate different, realistic constellations of implants, such as two middle ear implants, spinal cord stimulator and middle ear implant, integrated in a single phantom. In this document the following demonstrators for multi-implant MRI coexistence are shown:

- Prototype of spinal cord simulator
- Prototype of middle ear implant
- Multi-implant EM simulations
- Multi-implant RF heating bench test
- Multi-implant image distortion bench test

3. Prototypes for multi-implant assessment

3.1 Spinal cord stimulator

G-Therapeutics (GTX) is developing the Go-2 Targeted Epidural Spinal Stimulation (TESS) therapy to restore the ability to walk in people who suffered from spinal cord injury (SCI). The therapy combines an implantable neuro-stimulation system with real-time motion feedback with an intensive rehabilitation program (e.g. using body weight-assisted training tools) (Figure 1). The implantable neuro-stimulation system features a paddle lead electrode array with 16-channels implanted in the epidural space and an implantable pulse generator (IPG) that delivers electrical stimulation to the electrodes.

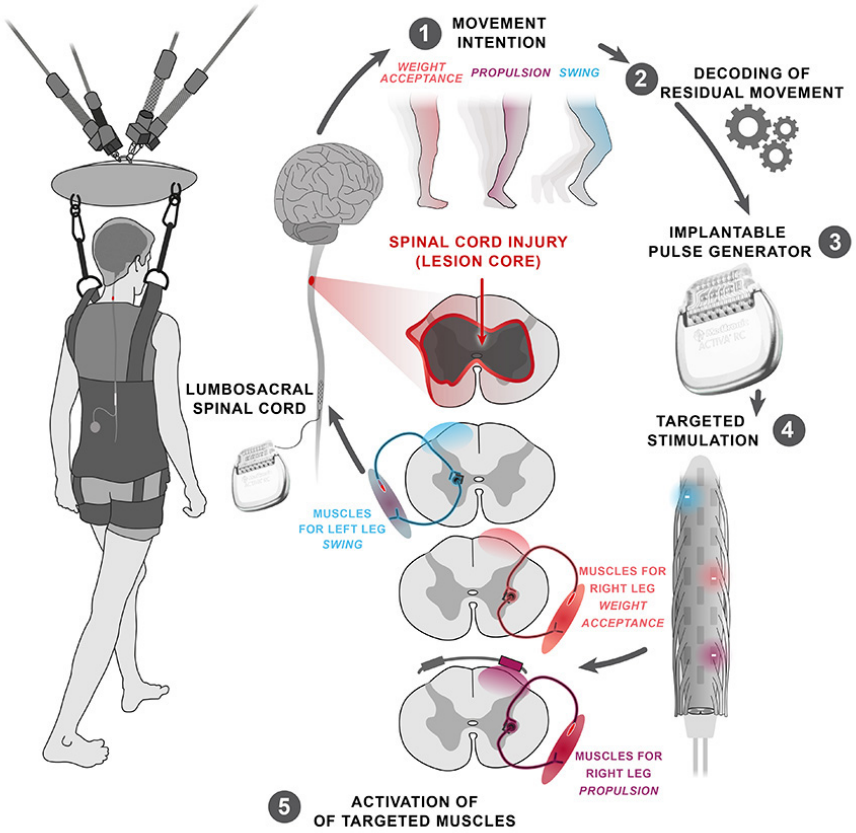

Figure 1: GTX system

Prototypes of the GTX electrode array have been manufactured and are tested for RF heating and image distortion in the MR environment (Section 5). The GTX IPG is not available for testing yet and therefore, the GTX lead will be connected to the compatible Medtronic Prime Advanced IPG.

3.2 Middle ear implant

The Cochlear™ Carina® implant is a fully-implantable middle ear implant (MEI) for patients with moderate to severe sensorineural, conductive or mixed hearing loss. The Carina MEI features a sensitive implantable microphone to pick up sound which is amplified in the implant body and converted into mechanical vibrations by the implantable actuator to stimulate a patient. Depending on a patient's specific needs, the actuator can be coupled to the ossicles, the oval window or the round window to compensate for the hearing loss.

In normal operation, the Carina system works as follows (Figure 2):

1. The implantable microphone (1) captures sound through the skin and sends it to the implant body (2)
2. Inside, the sound gets processed after which an electrical signal is generated
3. The signal gets transferred to the T2 middle ear actuator (3) coupled to the patient's middle ear structures (4)

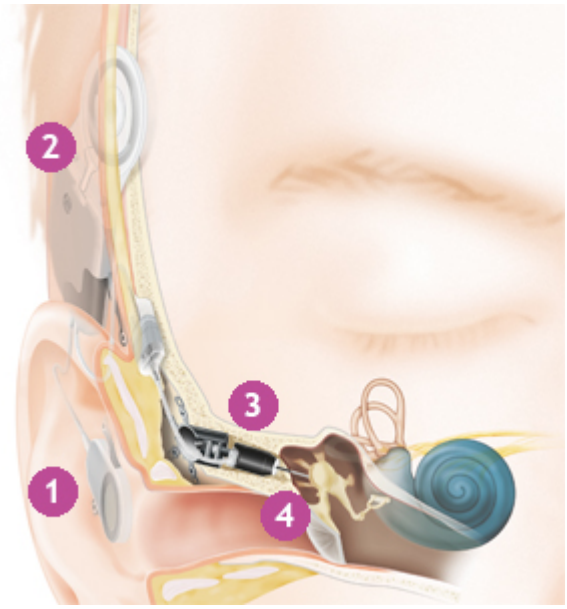

Figure 2: Schematic overview of the Carina system

The implant body also features an implanted coil and a retention magnet (Figure 3) for coupling the implant with the battery charger and with external accessories like the button audio processor to improve hearing in noisy environments.

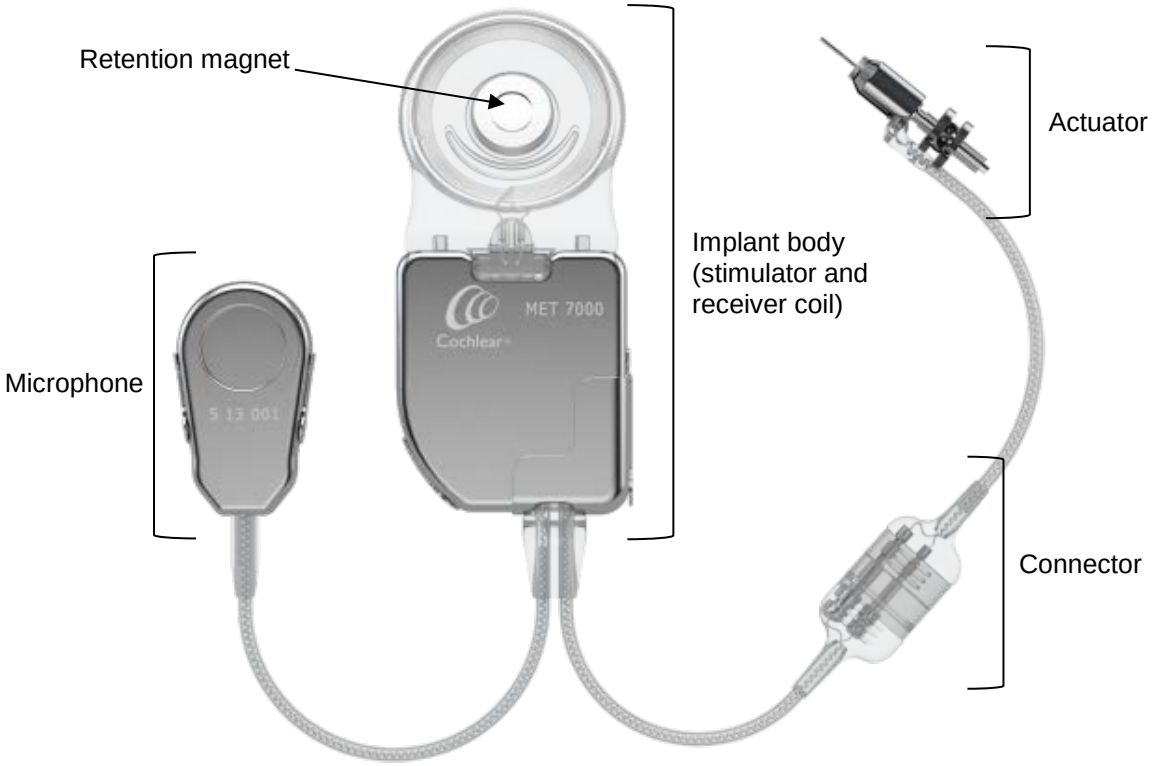

Figure 3: Carina implant

3.3 Phantom

The prototypes of the spinal cord stimulator and middle ear implant are tested in a Poly(methyl methacrylate) elliptical ASTM phantom with size of 650 x 420mm, 200mm radius, and 90mm liquid depth, as shown in Figure 4.

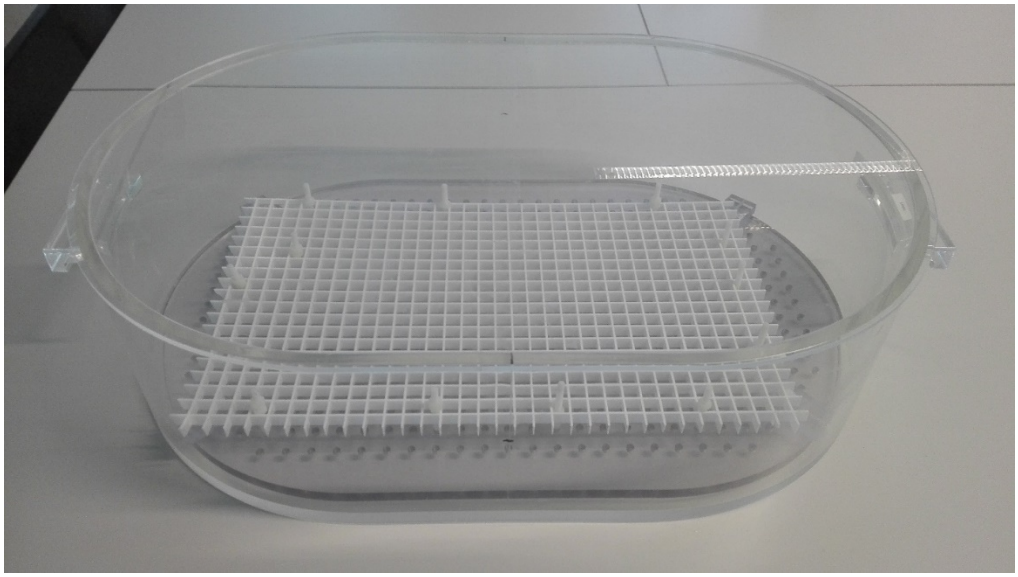

Figure 4: Elliptical ASTM phantom

4. EM simulations

In this section the EM simulations for multi implant assessment are described. Simulations were performed with Sim4Life, a platform developed by ZMT, Zurich, based on the finite-difference time-domain method (FDTD) [1].

4.1 MRI RF Coil

Figure 5 shows the CAD model for the Philips Ingenia 1.5T MRI system. Only the RF coil and RF shield are modelled. The RF coil is a 64 MHz high-pass 16 rung coil of 58 cm length.

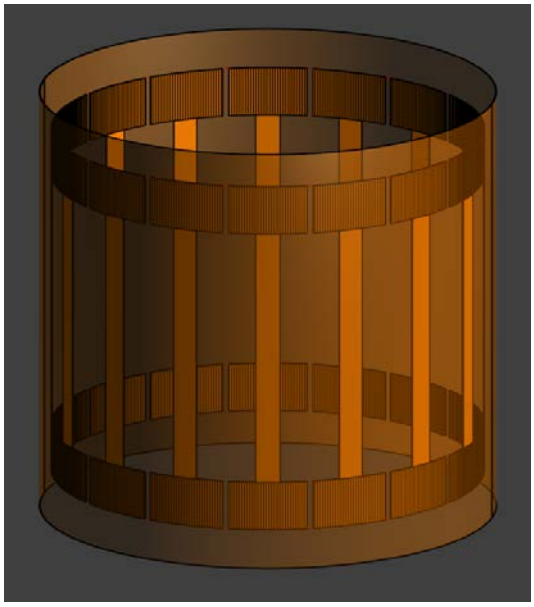

Figure 5: Philips Ingenia 1.5T RF coil and RF shield

4.1.1 Unloaded coil

The B1 field of the unloaded coil (i.e. empty) coil is shown in Figure 6. As desired, the $B1^+$ is homogenous around the isocentre and significantly larger than the opposingly rotating $B1^-$.

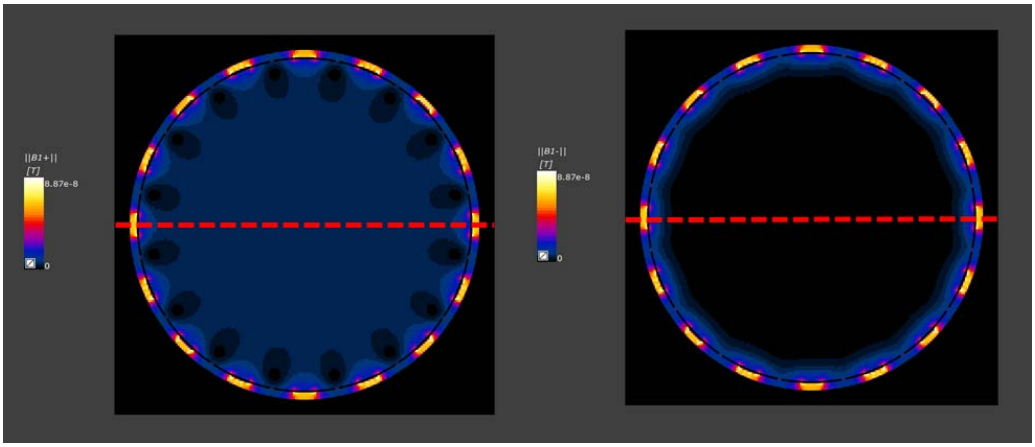

Figure 6: B1+ (left) and B1- (right) field at the coil isocentre. Coil is empty.

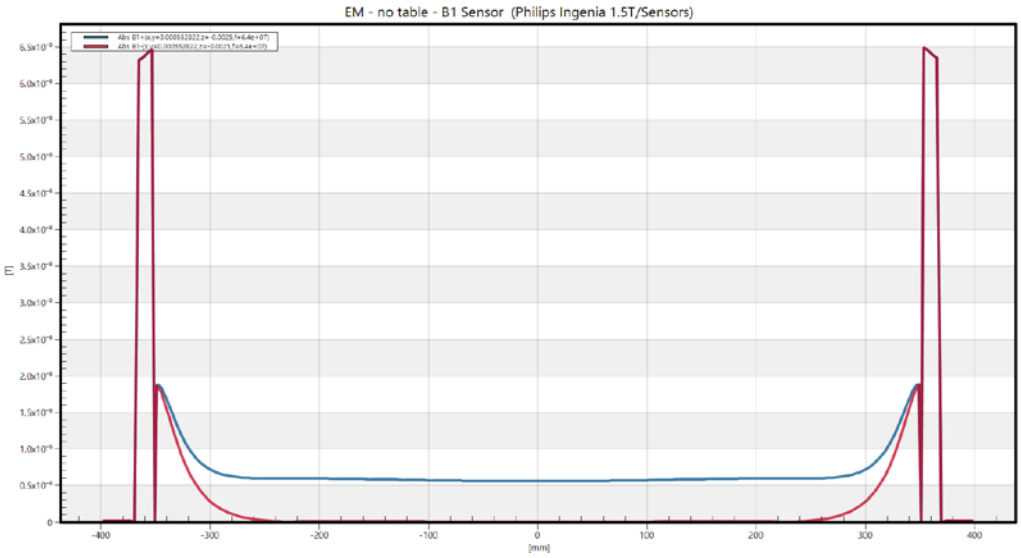

Figure 7: B1+ (blue) and B1- (red) field at the coil isocentre extracted along the dashed red line in Figure 6.

4.1.2 Loaded coil

Loading the coil with the elliptical phantom affects the homogeneity of B1 field (Figure 9 and Figure 10). The electric field (RMS values) induced in the phantom is shown in Figure 11 and Figure 12. The field distribution appears asymmetrical and the electric field is larger at the sides of the phantom.

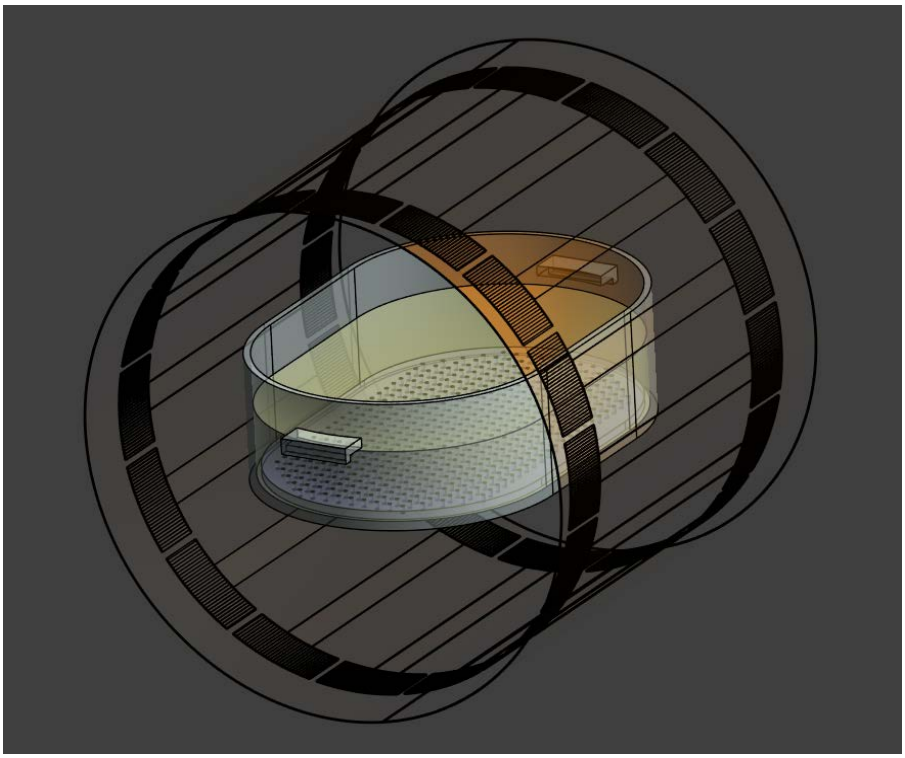

Figure 8: Elliptical ASTM phantom placed inside the coil.

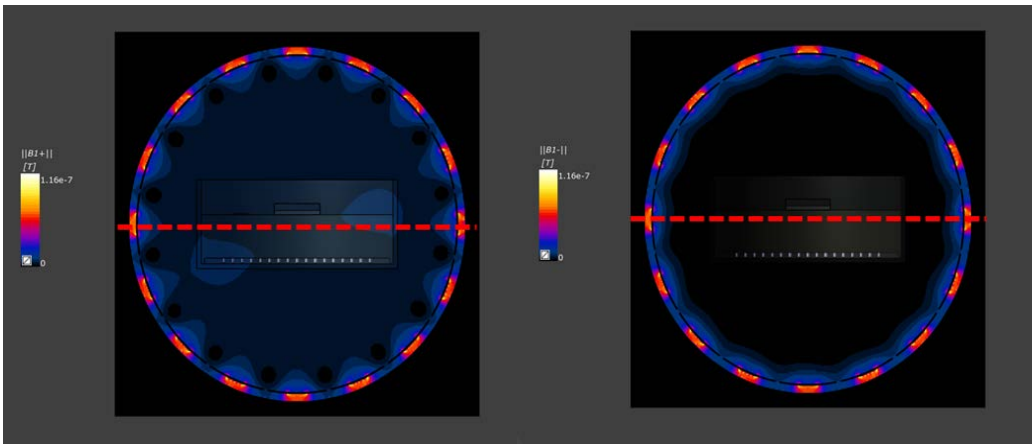

Figure 9: B1+ (left) and B1- (right) field at the coil isocentre. Coil is loaded with the phantom.

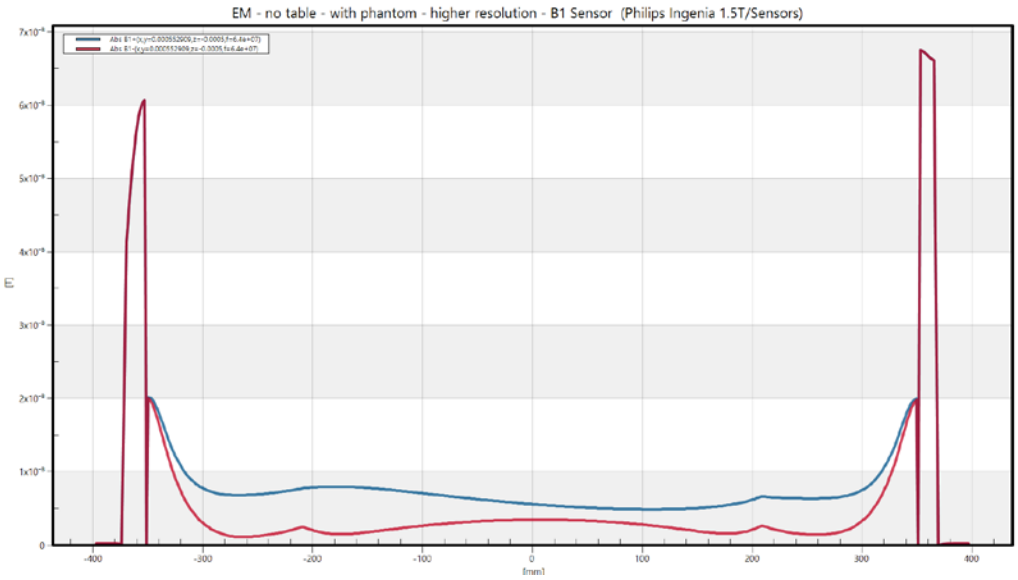

Figure 10: B1+ (blue) and B1- (red) field at the coil isocentre extracted along the dashed red line in Figure 9.

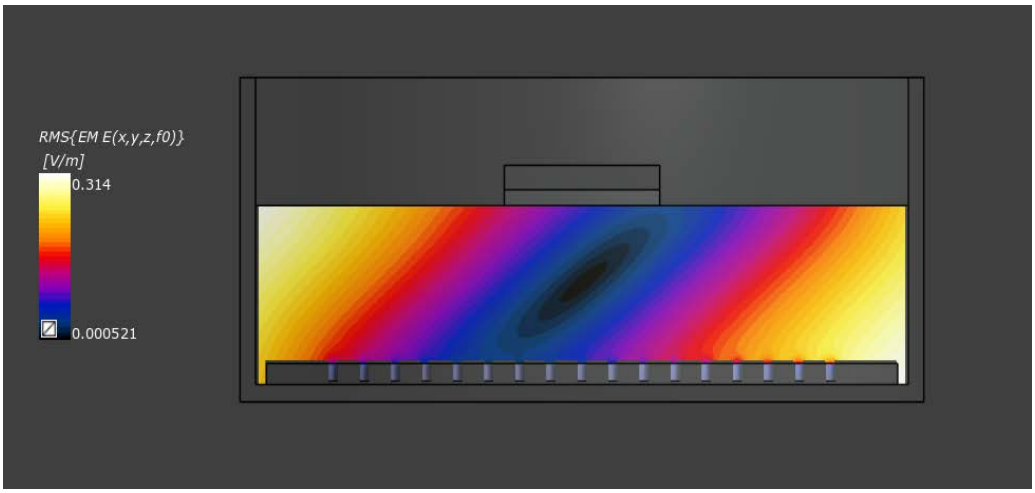

Figure 11: Coronal view of the electric field (RMS) inside the phantom.

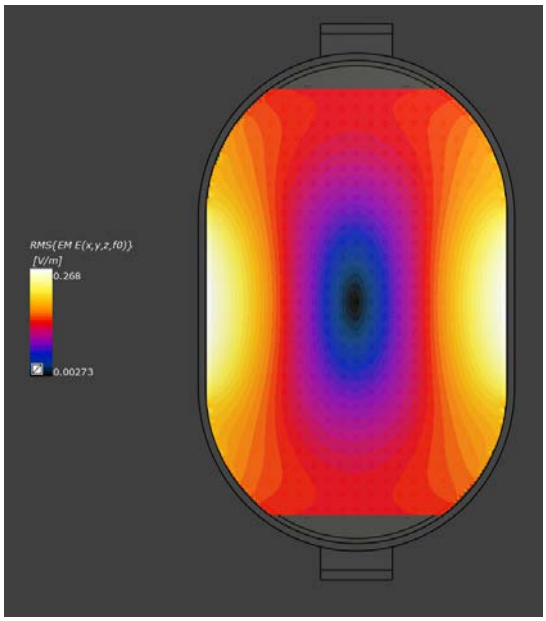

Figure 12: Axial view of the electric field (RMS) inside the phantom.

4.2 Multiple implants in elliptical ASTM phantom

4.2.1 Setup

Simplified models of the spinal cord stimulator and middle ear implant were created and placed in the phantom filled with HydroxyEthyl Cellulose (HEC) gel (σ=0.47 S/m, ε_r=78). Two inter-implant distances (4.5 and 9 cm) at three different landmarks (+15, 0 and -15 cm) i.e. location of the phantom in the MRI coil were simulated (Figure 13). The computational grid was generated for the scenario of both implants in the phantom and fixed for the scenario of individual implants to avoid additional uncertainty due to different grid settings between simulations.

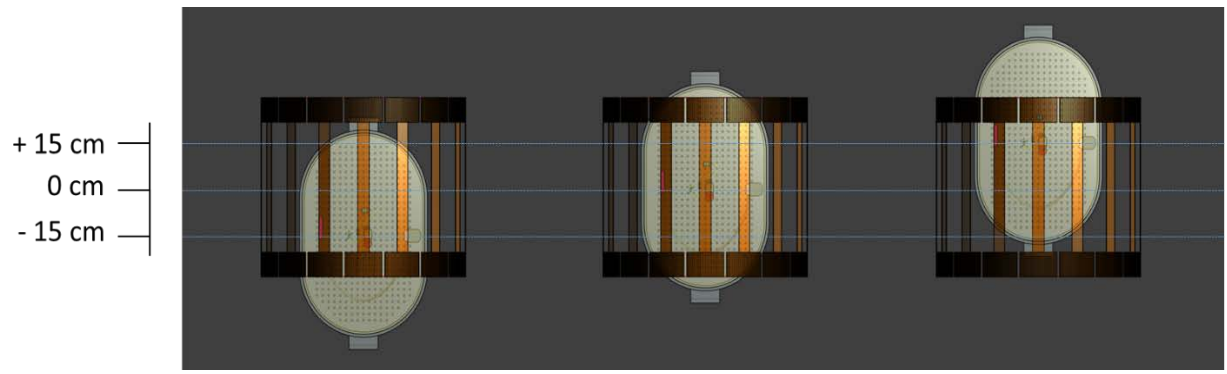

Figure 13: Landmarks of +15, 0 and -15 cm in the coil.

4.2.2 Fields

Results are provided in terms of specific absorption rate (SAR) distribution since this is correlated to the temperature increase [2]. Figure 14 shows the SAR distribution in the phantom due to the presence of the SCS. A localized increase of SAR at the SCS electrodes can be observed, even if the lead and IPG locations are reversed. The focus is on assessing how the maximum value of SAR changes when the middle ear implant is placed near the SCS as in Figure 15 rather than on the absolute values. In addition, the simulations were repeated for the scenario of two nearby middle ear implants (Figure 16).

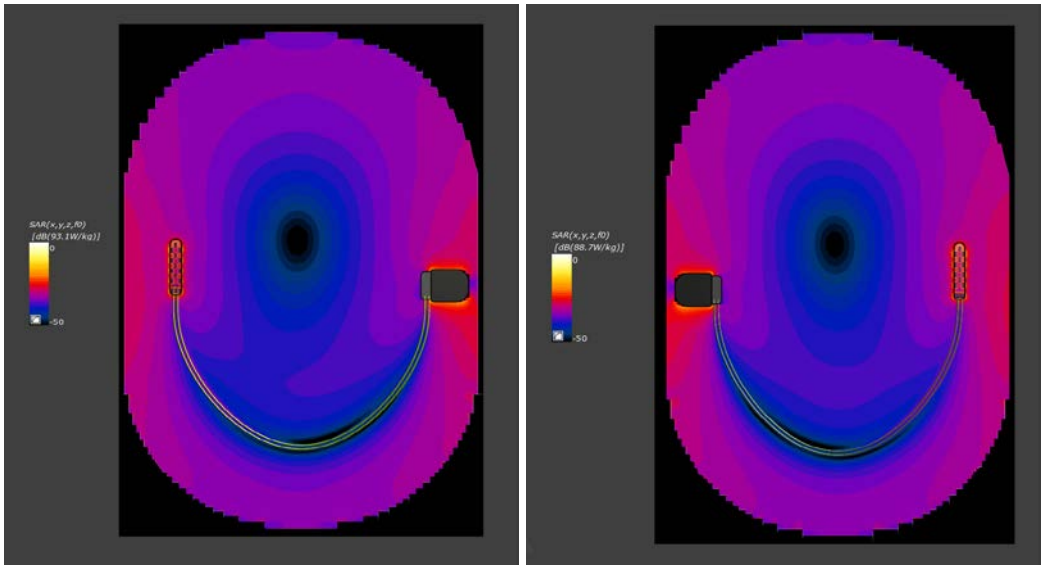

Figure 14: SAR field for the SCS at landmark 0 cm. On the right hand-side, location of the SCS lead and IPG have been reversed.

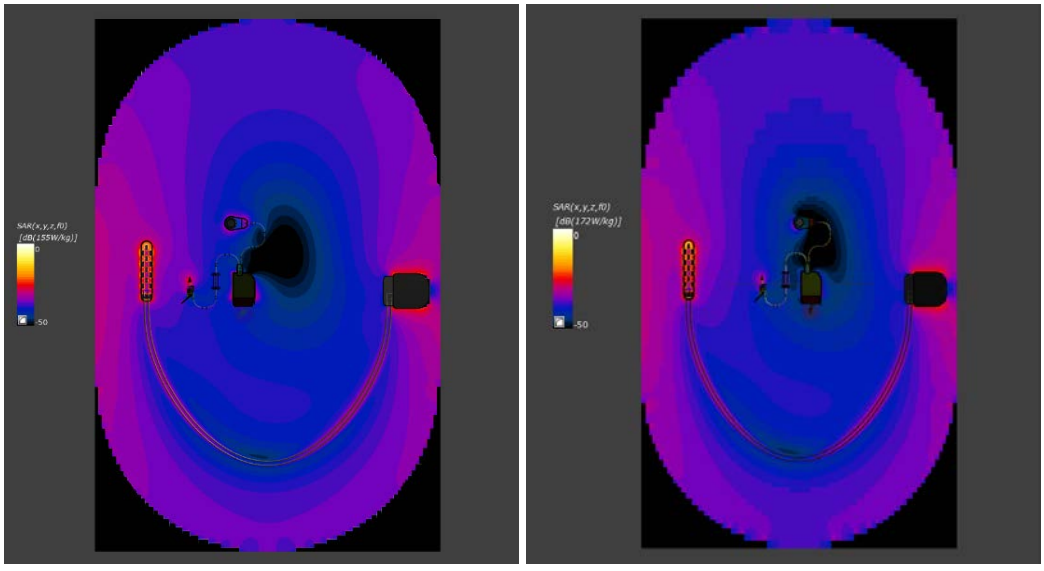

Figure 15: SAR field for the SCS and middle ear implant at landmark 0 cm. Inter-implant distance is 4.5 cm (left hand-side) and 9 cm (right hand-side).

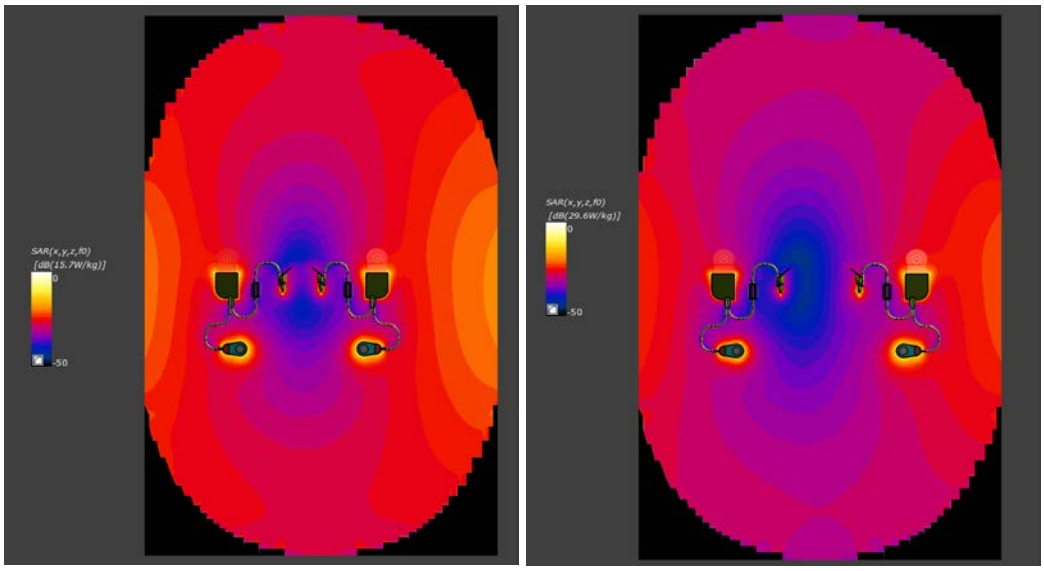

Figure 16: SAR field for the two middle ear implants at landmark 0 cm. Inter-implant distance is 4.5 cm (left hand-side) and 9 cm (right hand-side).

4.2.3 Max SAR

Results for the estimated max SAR are plotted in Figure 17 and Figure 18 for the SCS and middle ear implant and for two middle ear implants, respectively. The SAR values are normalized to 1W input power. For the scenario of the SCS and the middle ear implant, the peak SAR was observed at the electrodes of the SCS lead. No significant difference was observed between the SCS only and the SCS together with the middle ear implant at inter-implant distance of 9 cm (<1%). The largest percentage difference was observed for inter-implant distance of 4.5 cm at landmark 0 (SAR ~10% lower for multiple implant scenario). For the simulations with two middle ear implants, SAR values were always lower for the multi-implant than the single implant scenario. The largest percentage difference was observed for inter-implant distance of 9 cm at landmark -15 cm (SAR ~17% lower for multiple implant scenario).

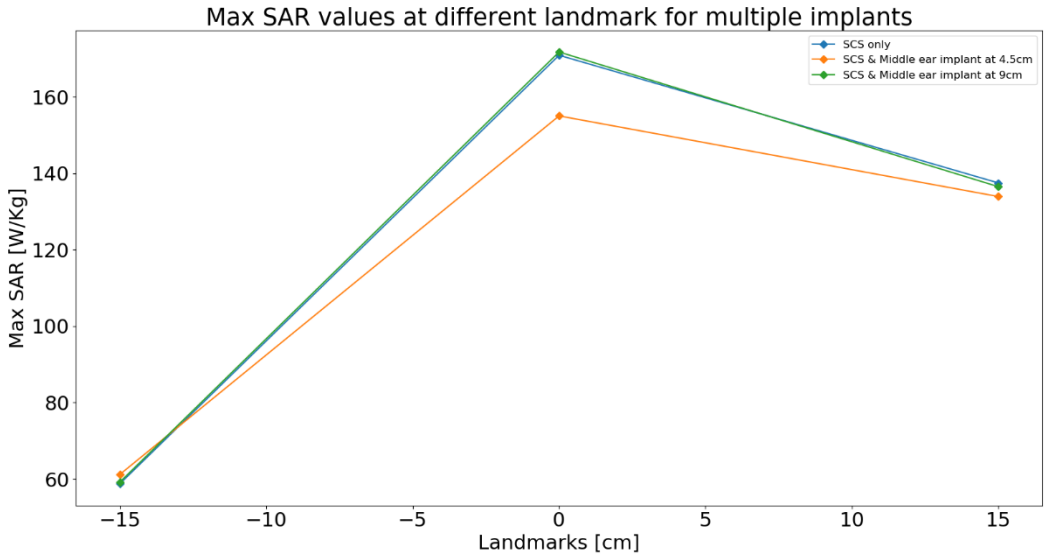

Figure 17: Max SAR for SCS and middle ear implant at different landmarks in the coil. Values are normalized to 1W input power.

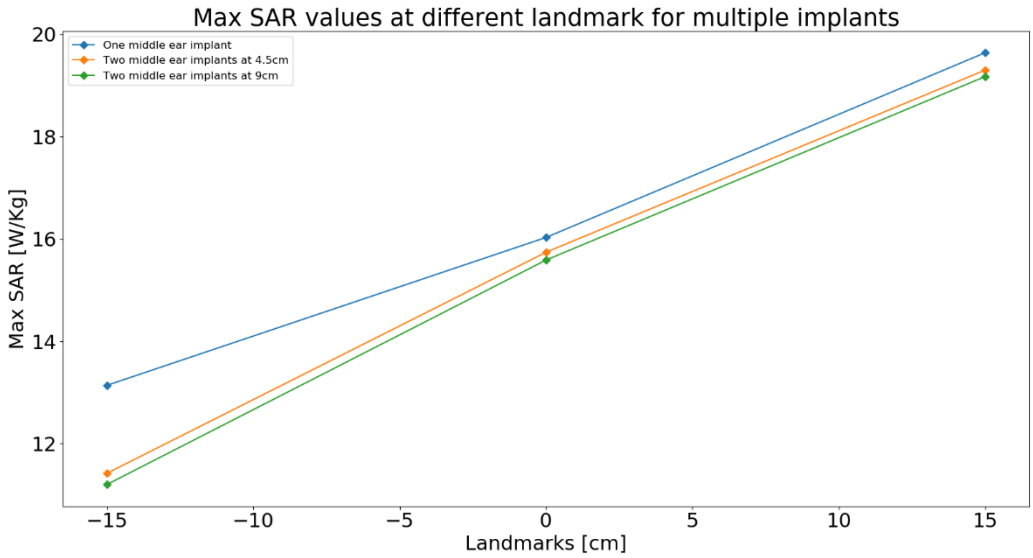

Figure 18: Max SAR for two middle ear implants at different landmarks in the coil. Values are normalized to 1W input power.

4.3 Generic leads in Virtual Population model

The preliminary results for multi-implant assessment in a more realistic human model are presented here. The SCS and middle ear implants were further simplified down to generic AIMD leads and positioned according to representative routings (Figure 19). Specifically, the SCS is modelled as an insulated 320 mm long, 1.5 mm radius wire with an insulation radius of 2.5 mm and the middle ear implant is modelled as an insulated 96 mm long, 1.5 mm radius wire with an insulation radius of 2.5 mm. Both wires have a 10 mm long bare segment at the ends. RF heating was evaluated for an adult male Duke model of the Virtual Population [3] at two landmarks in the coil (Figure 20). Three scenarios were simulated:

1. Duke with SCS generic lead only
2. Duke with middle ear implant generic only
3. Duke with both generic implants

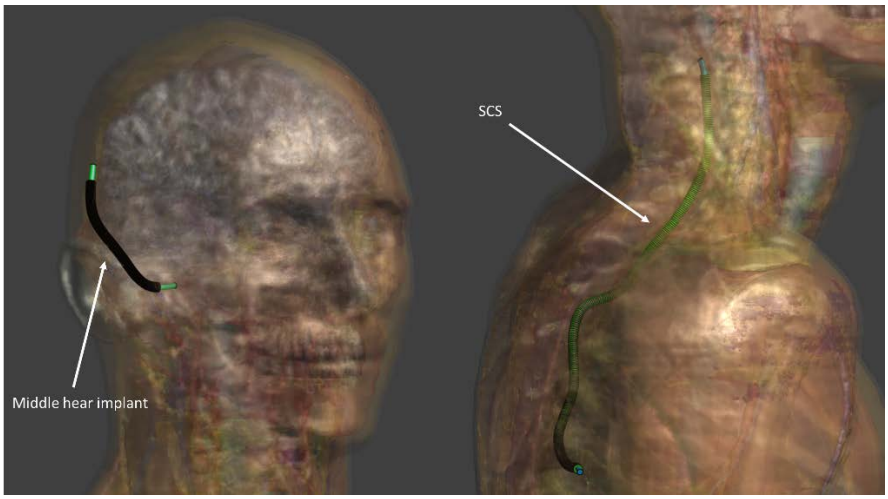

Figure 19: Generic leads in Duke model from the virtual population.

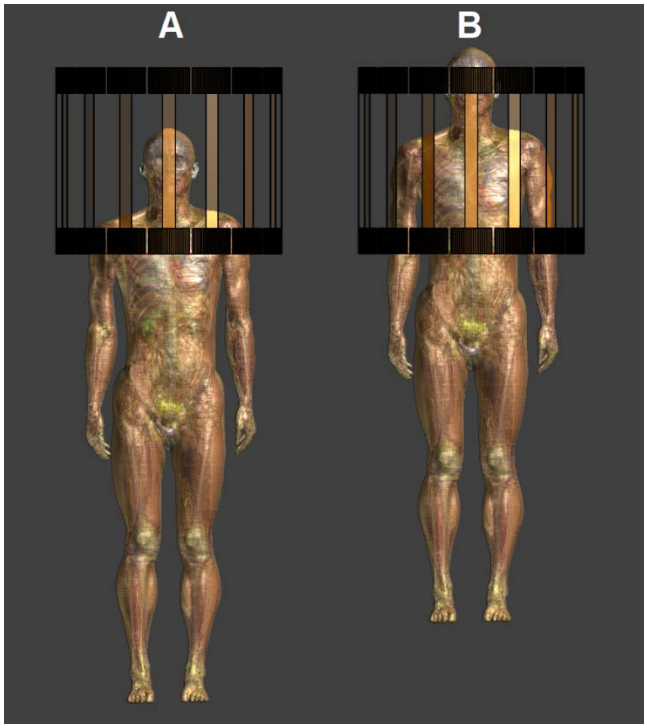

Figure 20: Duke model from the virtual population at the two landmarks in the coil. For Landmark A Duke's head is at the MRI coil isocentre, whereas for Landmark B Duke's torso is at the MRI coil isocentre.

4.3.1 Fields

Figure 21, Figure 22 and Figure 23 show the SAR distribution for the tissues near the implants' tip. A localized increase of SAR due to the power deposition by the implants can be observed.

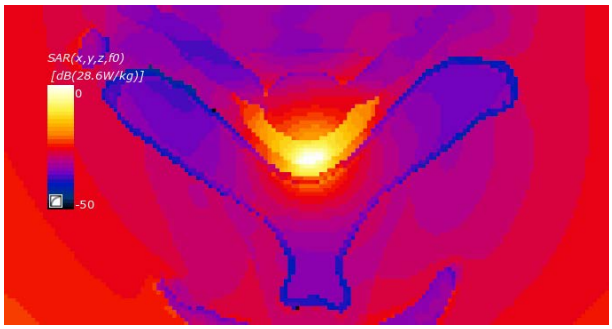

Figure 21: Axial view of localized SAR increase at SCS generic lead in Duke model at landmark A.

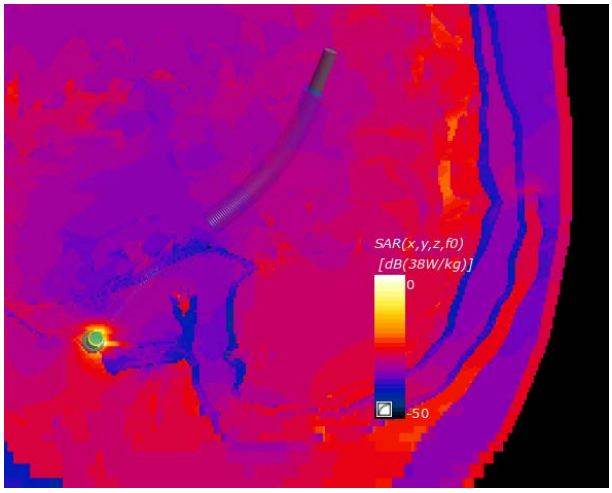

Figure 22: Sagittal view of localized SAR increase at middle ear implant generic lead tip in Duke model at landmark A.

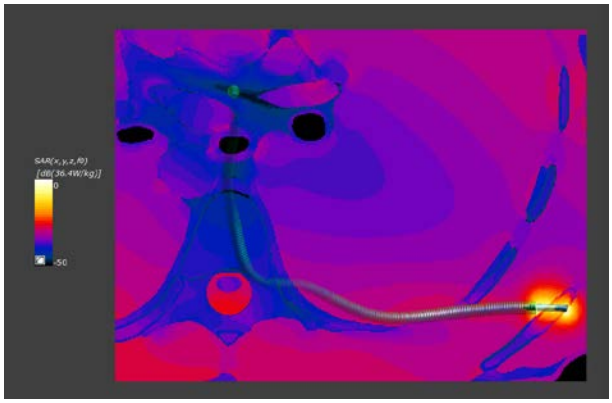

Figure 23: Axial view of localized SAR increase at SCS generic lead in Duke model at landmark B.

4.3.2 Max SAR

Results for the estimated max SAR for the SCS and middle ear implant in Duke are plotted in Figure 24, and Figure 25, respectively. SAR values of the single implant scenario are compared with the multiple implants' scenario. SAR values are normalized for 1W input power. For landmark A the peak SAR was observed at the middle ear implant generic lead, while for landmark B the peak SAR was observed at the SCS generic lead. It can be observed that the presence of the other implant did not affect significantly the max SAR value (<0.02% difference).

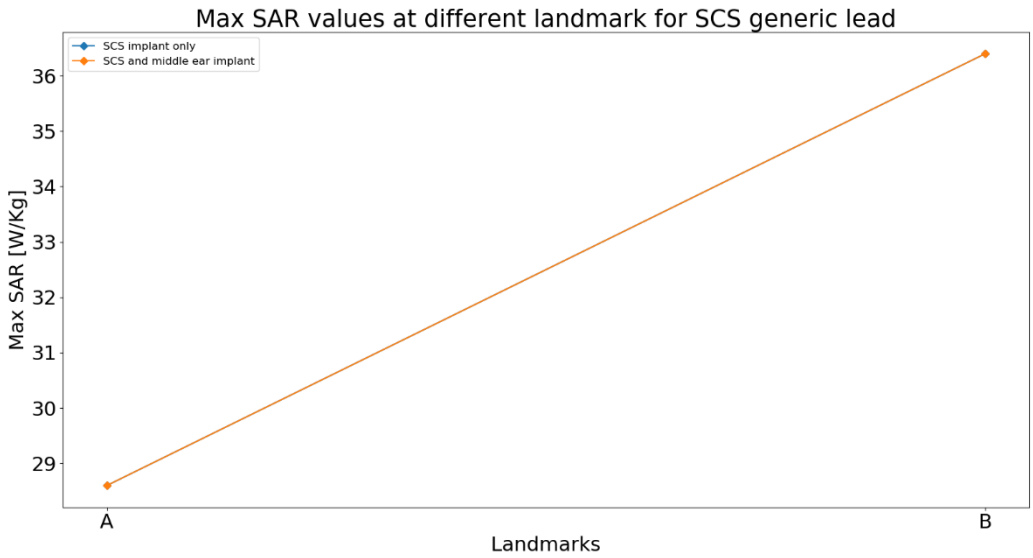

Figure 24: Max SAR for SCS generic lead in Duke model at different landmarks.

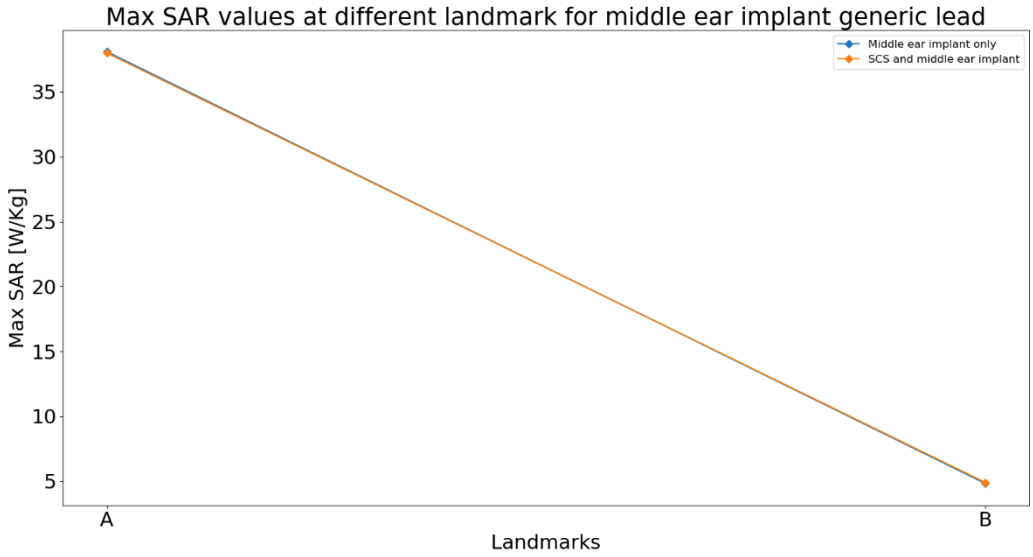

Figure 25: Max SAR for middle ear implant generic lead in Duke model at different landmarks.

5. Bench tests

5.1 RF Heating

5.1.1 Equipment

Table 1: Equipment used during RF heating tests

Equipment Description	Quantity	Comments
MRI scanner	1 pc	Philips Ingenia 1.5T
Phantom	1 pc	As described in paragraph 3.3
Tissue simulating medium	1 pc	As described in paragraph 5.1.2
Implant attachments	>20 pcs	Different 3D-printed parts that simplify positioning the different implants inside the phantom
Temperature sensors	9 pcs	Four FISO THR-NS-1165F fiber optic temperature sensors are provided for each implant. In addition, 1 sensor is used to provide baseline measurements
Signal conditioner	5 pcs	Five FISO SPC-HR-NS-882A dual-channel signal conditioner modules
Signal conditioner modules mounting rack	1 pc	One FISO EVO-SD-5 mounting rack is used to mount the signal conditioner modules

5.1.2 Phantom preparation

A phantom containing a tissue simulating medium is prepared as described in annex L of ISO/TS 10974 (2018) [4]. The gel material is made in a separate container before the start of the experiment and consists of a mixture of 96.85 % water, 3% Hydroxyethyl Cellulose (HEC) and 0.15% NaCl, resulting in a relative dielectric permittivity of 78 and a conductivity of 0.47 S/m which is a high permittivity medium (simulating the immediate surroundings of the implant) with an electrical conductivity simulating the global average of biological tissues).

The implant(s) are mounted in the empty phantom in a similar way as they are modelled (Section 4). Based on the simulation results described in paragraph 4.2.2, temperature sensors are mounted in close proximity to the calculated hotspots. A minimum positioning accuracy of 0.25 mm with respect to the implant hotspot is maintained as prescribed in clause 8 of ISO/TS 10974 [4] for SAR-based simulations. In addition, an additional temperature sensor is mounted at least 10 cm away from the implant(s) to measure background heating.

Once the implant(s) and temperature sensors are mounted inside the empty phantom, the phantom is put on the patient bed inside the MRI suite, after which it is filled with the tissue simulating medium. Finally, the phantom is moved forward into the patient bore for scanning in the different simulated positions (Section 4).

5.1.3 Scanning and data acquisition

Measurement data from the temperature sensors is acquired via the Evolution software (FISO Technologies, Quebec, CA) package provided with the sensors.

Different clinical scan examinations will be tested consisting of different sequences, with the emphasis on worst case sequences with a high level of deposed RF energy (Table 2).

Table 2: Example scan sequences used during RF heating experiment

Sequence name	plane	Info
Localizer	3D	Gradient echo (Smart brain, Smart spine)
T2 MV	Axial	TSE sequence (high SAR) (Brain)
Diffusion	Axial	SE EPI sequence (low SAR) high dB/dT (Brain)
3D T2 FLAIR	3D Sagittal	Inversion recovery TSE sequence (high SAR) (Brain)
3D TOF Angio	3D Axial	Gradient echo (Brain)
3D Thrive	3D Sagittal	Gradient echo (Brain)
Perfusion	Axial	GE EPI Sequence (low SAR) high dB/dT (Brain)
T2 TSE	Sagittal	TSE sequence (high SAR) (Spine)
T2 TSE	Axial	TSE sequence (high SAR) (Spine)
T1 TSE	Sagittal	TSE sequence (high SAR) (Spine)

5.2 Image Distortion

5.2.1 Equipment

Table 3: Equipment used during image distortion testing

Equipment Description	Quantity	Comments
MRI scanner	1 pc	Philips Ingenia 1.5T
Phantom	1 pc	As described in paragraph 3.3
Tissue simulating medium	1 pc	As described in paragraph 5.1.2
Copper Sulphate Pentahydrate	60 g[1]	Fagron product number 0318113
Implant attachments	>20 pcs	Different 3D-printed parts that simplify positioning the different implants inside the phantom

[1] Assuming a water content of at least 30 l in the phantom. This would lead to a CuSO4 concentration between 1-2 g/l as prescribed in ASTM F2119 [5]

5.2.2 Phantom preparation

The following procedure is followed to prepare the phantom for scanning:

1. Mount the implant(s) on the plastic grid in the phantom.
2. Put the empty phantom on the patient bed inside the MRI suite.
3. Fill the phantom with tap water until it has a content of at least 30 l.
4. Mix in the CuSO4.
5. Close the phantom with the accompanying lid.

Once the phantom is prepared it can be moved inside the scanner bore to a predefined position for scanning described in paragraph 5.2.3. Afterwards the phantom can be moved backwards so that the implant(s) can be removed. Afterwards additional images are acquired without the implant(s) to serve as reference images.

5.2.3 Scanning and data acquisition

Distortion test scans are being acquired using several different sequences which are both sensitive to distortion (gradient echo scans) and less sensitive to distortion (spin echo scans) and special sequences to minimize distortion such as:

- View angle tilting scans (VAT).
- Slice encoding for Metal Artefact Correction sequences (SEMAC).
- Metal artefact reduction scans (MARS) consisting of high bandwidth high resolution scans.
- A combination of the above techniques.

6. Conclusions

In this deliverable, the demonstrators realised in WP2 of the DISPERSE project have been described. Prototypes of the GTX SCS system and Cochlear™ Carina® implant were presented. These implants have been used to preliminarily assess multi-implant MRI coexistence both in-silico and in-vitro. EM simulations for different implant configurations in a phantom have been performed and the peak SAR values were evaluated. Results for the investigated configurations showed that multi-implant scenario generally leads to a lower peak SAR value than the single implant scenario. Nonetheless, the limited number of landmarks and implant trajectories tested makes the generalization of these findings difficult. Simulations in a more realistic human phantom were also performed with two generic leads placed along representative trajectories for SCS and MEI implants. No significant difference in the SAR values for the multi-implant and single implant scenario was observed most likely due to the larger distance between the implants that reduced their interaction. Finally, the setup for RF heating and image distortion phantom experiments were described. The experiments will be soon performed to further study the multi-plant MRI coexistence and validate the results of the in-silico investigation.

7. References

[1] A. Taflove and S. Hagness, Computational electromagnetics: The finite-difference time-domain method, 2nd ed., Boston; London: Artech House, 2000.

[2] P. S. K. R. A. A. S. F. Nyenhuis J, “MRI and implanted medical devices: Basic,” *IEEE Trans Device Mater Rel,* vol. 5, no. 3, p. 467–480, 2005.

[3] M. C. Gosselin, E. Neufeld, H. Moser, E. Huber, S. Farcito, L. Gerber, M. Jedensjö, I. Hilber, F. Di Gennaro, B. Lloyd, E. Cherubini, D. Szczerba, W. Kainz and N. Kuster, “Development of a new generation of high-resolution anatomical models for medical device evaluation: the Virtual Population 3.0.,” *Physics in Medicine & Biology,* vol. 59, no. 18, 2014.

[4] ISO, ISO/TS 10974: Assessment of the safety of magnetic resonance imaging for patients with an active implantable medical device, International Organization for Standardization, 2018.

[5] ASTM International, F2119-07: Standard Test Method for Evaluation of MR Image Artifacts from Passive Implants, ASTM International, 2013.